Proceedings of ASME Turbo Expo 2022
Turbomachinery Technical Conference and Exposition
GT2022
June 13-17, 2022, Rotterdam, The Netherlands

GT2022-84165

PREDICTING CAVITATION EROSION ON TWO-STAGE PUMPS USING CFD

Tedja Verhulst
Cranfield University
Cranfield, UK

Eddie Yin-Kwee Ng
Nanyang Technological University,
Singapore

Yongmann Chung
University of Warwick
Coventry, UK

David Judt
Cranfield University
Cranfield, UK

Craig Lawson
Cranfield University
Cranfield, UK

ABSTRACT

Cavitation is a common problem that occurs in pumps which reduces its useful life and bring increased operating costs to the user. A study of cavitation erosion on a two-stage centrifugal pump has been carried out using Computational Fluid Dynamics (CFD). Most cavitation studies on pumps have been focused on modelling the severity of cavitation; specifically, on understanding its visual effects and performance penalties. Few works have been carried out to predict the most erosion-sensitive areas inside a pump. The focus of this study is on modelling the permanent damage that would be caused by cavitation and to identify specific areas within the pump which are most susceptible to erosion. The model is first validated against experimental data from another work. Once the simulation has been successfully calibrated, the cavitation simulation is carried out again with the subject pump. Not only does this work extend the findings previous works by predicting cavitation erosion on a two-stage pump, but the pump rotation speed is also varied to observe how the erosion-sensitive areas on the pump changes as a result. A specific focus on the Gray Level Method is carried out to predict the erosion damage on the pump. This technique is chosen as it has been experimentally proven with single-stage radial pumps, using specialized CFD code. It is found that the algorithm used to predict erosion when applied with commercial CFD packages, are useful in distinguishing areas inside the pump which are most vulnerable to erosion damage. The Scherr-Sauer cavitation model coupled with the κ-ω SST turbulence model have been used to run the cavitation simulations.

Keywords: Erosion, CFD, friction and wear, bubble growth, vaporization, centrifugal pumps and compressors.

NOMENCLATURE

List of key terms, acronyms and its symbol:

σ	Cavitation number	-
ρ	Density	kg/m^3
ρ_l	Liquid Density	kg/m^3
α	Vapor Fraction	-
P	Pressure	Pa
Q	Flowrate	kg/s
P_v	Saturation Pressure	Pa
v	Velocity	m/s
t	Time	s
Δt	Time-step duration	s
T	Incubation time	s
v_{jet}	Jet velocity	m/s
v_{crit}	Critical velocity	m/s
v_{def}	Deformation Velocity	m/s
A_{pit}	Pit area	mm
A_{ref}	Reference Area	mm
A_{dam}	Damaged Area	%
R_b	Bubble Radius	m
N_b	Bubble Density	m^3
c	Chord/Radial length	mm
GCI	Grid Convergence Index	%
p	Local Order of Accuracy	-
LE/TE	Leading/Trailing Edge	
CFD	Computational Fluid Dynamics	
Star-CCM+	CFD Software Package	
CFturbo	Pump Design Software Package	
GLM	Gray Level Method	
IFM	Intensity Function Method	
EPM	Erosion Power Method	
DBM	Direct Bubble Method	
κ-ε	Kappa-Epsilon Turbulence Model	
κ-ω	Kappa-Omega Turbulence Model	
SST	Shear-Stress Transport Turbulence Model	

1. INTRODUCTION

Cavitation is a common problem found in pumps across different industries. This phenomenon can not only reduce the performance of the pump, but significantly cost the operator financial losses due to premature pump failures and the pump being replaced earlier than intended, as it can no longer produce the required head. Cavitation does not only occur in pump impellers, but also occurs in other blade applications such as hydrofoils and propellers. It is therefore useful to predict for cavitation erosion and to understand how it would damage the pump. Having the ability to predict this fault is useful as it allows pump designers to apply design improvements to prolong its useful life. Operators can also benefit as it gives them the ability to apply corrective action for the pumps and help mitigate the financial penalties associated with unexpected breakdowns.

In order to predict the pump erosion from cavitation, a simulation using a multiphase fluid model of water is used to stimulate cavitation on the pump, executed using Computational Fluid Dynamics (CFD). CFD refers to the branch in fluid mechanics that uses numerical analysis to solve problems that involve fluid flows and its interaction with surfaces. CFD methods are chosen to predict erosion as it is a low-cost, time-efficient alternative over stimulating cavitation naturally with a test rig, and allows the problem to be visualized in software. The results from this simulation can help identify specific areas inside the pump that are most vulnerable to cavitation damage.

Previous works on cavitation simulations on CFD have been focused on the visual study of the vapor fractions and how it influences the pump performance. Very few works have attempted to predict the regions inside the pump that are affected by erosion damage. Authors in previous works such as [1, 2, 3, 4, 5] have studied cavitation on a two-sta ge pump, but has not made an attempt to create a model that predicts where the erosion damage would occur. Similarly, previous works such as by Dular et al [6], Usta et al. [7] as well as Li and Van Terswiga [8] have respectively developed the field functions to predict erosion and tested it on single-stage pumps, propellers and aerofoils, but none has carried out the same study on a two-stage centrifugal pump. These specifically developed field functions allows the erosion-sensitive areas to be highlighted in the simulation and is called Gray Level Method (GLM), it relies on calculating some function of the pressure value, derived from the parameters calculated while running the cavitation model. Other methods such as the maximum pressure, intensity function, erosive power and direct bubble methods have been considered, but are not included as they have not been experimentally validated against a radial pump.

The main objective of this paper is to demonstrate cavitation erosion prediction using CFD for a two-stage pump, at different speeds, the GLM erosion function. The results from the simulations can be used to estimate the damage caused by cavitation erosion to a pump with a high degree of realism. An overview of existing works related to modelling cavitation erosion is first carried out. The second part focuses on the overall methodology and how the simulation is set-up using CFD. The third part focuses on calibrating the CFD simulation with a reference experiment so that the predictions are accurate. Finally, the verified erosion model is applied to a two-stage impeller pump. Since there are two pumps mentioned, the pump used to calibrate the cavitation model is called the reference pump, and two-stage pump that will be the focus of this paper is called the subject pump. The type of pump used for both simulations is a centrifugal pump with a radial impeller. For simplification, this is called a radial pump throughout the rest of the paper. The simulation is tested at different rotational speeds of the pump, so that the relationship between pump rotation speed and areas affected by erosion can be appreciated. Prior to the cavitation simulations, the performance of the subject pump is validated under non-cavitating conditions against the manufacturer datasheet. The focus of the erosion wear analyses is on the impeller blades, as there are no experimental data that exist for the other pump components.

2. LITERATURE REVIEW

To understand the mechanism of cavitation erosion damage, the cavitation theory must first be understood. The erosion models leverage variables extracted from the cavitation simulation in CFD to predict the erosion areas. The cavitation theory that underpins the erosion prediction helps to understand how the boundary conditions are configured in simulation.

2.1 Cavitation Theory

Cavitation occurs when the pressure observed at the pump inlet is less than the vapor pressure of the liquid. For a pump, the leading edge of the impeller is considered to be the most vulnerable region, as this is the point at which the static pressure is the lowest in the entire pump [9]. This creates bubbles in a trail of vapor which reduces the head output of the pump. Furthermore, these bubbles implode at very high pressures as it travels towards the trailing of the pump impeller which creates an erosive effect on the metal surface. This results to permanent damage to the pump impeller and reduces its capability to generate head at a given flowrate. If the erosion becomes severe, then the pump can no longer produce the required head to be useful or fail altogether. Cavitation for pumps is a transient behavior, where the cavitation appears briefly when the boundary conditions are satisfied and eventually disappears when the pump reaches steady state boost pressure [10, 11].

The actual value of this vapor pressure is dependent on the temperature, altitude and the type of fluid being pumped. Water (H_2O) at sea level and room temperature has a vapor pressure of 3170 Pa but this threshold can increase if the ambient temperature or altitude is raised, making the pump more susceptible to cavitation. A non-dimensionless parameter which gives an indication to the severity of cavitation is called the cavitation number. The lower this value, the more severe the cavitation. The cavitation number is defined as follows [12]:

$$\sigma = \frac{P_T - P_v}{\frac{3}{4}\rho_l v^2} \quad (1)$$

For Eq. (1), σ Refers to the cavitation number, P_T is the total pressure measured at the pump inlet, P_v is the vapour pressure of fluid, ρ_l density of the liquid and v rotation velocity of the pump impeller. For a hydrofoil, the constant on the denominator is $\frac{1}{2}$ instead of $\frac{3}{4}$ [6]. The thresholds for the severity cavitation are dependent on the application of the blade. An example of this with a hydrofoil, where a value of $\sigma < 3$ is considered to be severe whereas for pump impellers this value is $\sigma < 0.5$.

The damage mechanism caused by cavitation erosion creates a sandpaper-like surface on specific regions of the pump such as the impeller. The effects of pump erosion have been known to reduce the its capability to boost pressure and compromise operational efficiency, as highlighted by the works by the various authors to evaluate for erosion damage to pumps in [13, 14, 15, 16, 17, 18, 19, 20]. When the erosion becomes severe, the pump can no longer operate effectively or fails completely altogether.

These works discuss the damage mechanism and performance penalties of erosion but the authors do not propose a mathematical model to predict it.

Vapor fraction α, is the most common parameter used to observe for cavitation in CFD and is useful to understanding areas in the pump where the bubbles grow and collapse, but does not highlight the areas that are affected by the subsequent erosion. This dimensionless parameter quantifies the ratio of vapor to liquid that is present in the fluid with a maximum value of 1 and minimum value of 0. An example of how vapor fraction is utilized to study cavitation is available in the works carried out by the authors [1, 2, 3, 4, 5] for two-stage pumps and [21, 22, 23] for single-stage pumps. The simulations carried out in these works focus on the visual study of cavitation for different blade geometries, but they do not give an in-depth explanation on how the erosion will develop as a result of cavitation.

2.2 Previous Works for Erosion Prediction

There have been past works which have modelled cavitation erosion using CFD for different types of blade applications, such as pump impellers, ship propellers and hydrfoils. These methods work by applying user-defined field functions to predict the areas where the erosion damage is most concentrated. Most of the used-defined field functions described are primarily based on some relationship with the changes in pressure caused by the cavitation process. The models leverage the assertion that the bubble collapse generates a pressure value that is much higher than the ambient pressure and that locations of these bubble implosions in turn are areas in the pump that have highest concentration of erosion [24, 25]. There is no single universal method that is able to predict erosion damage reliably for all applications and its accuracy will depend on the blade geometry. The variables used for the user-defined field functions have been calculated from the running of the cavitation simulation, so no additional model is required to apply them in predicting erosion.

The simplest out of the four erosion models discussed by the authors Schmidt et al [26] as well as Boorsma & Whitworth [27] uses the maximum pressure on the regions where the vapor fractions collapse on the surface to determine which parts of the pump are most sensitive to erosion. While this model is simple, it does not give an accurate approximation of the erosion areas.

The Intensity Function Method (IFM) was devised by Li & Van Terswiga [8] and applied to an aerofoil by Eskilsson & Bensow [28] as well as by Usta et al [7]. This method was devised to improve on estimating erosion areas using maximum pressure method, and relies on visualizing the pressure gradient on the surface and specific thresholds.

The Gray Level Method (GLM) outlined by Equation (2) was devised by Dular et al. [6] and has demonstrated its accuracy in predicting erosion on a single-stage radial pump and a hydrofoil. The more rigorous version of GLM is used in this work. Unlike all of the other methods mentioned, it is able to quantify the amount of erosion, in addition to identifying the areas. The more advanced implementation of GLM involves the calculation of jet velocities and associated deformation pressure on the pump surface, which is detailed further in sub-section 2.4.

The Erosive Power Method (EPM) was reported by Usta et al. [7] and has been further tested by [29] Koksal et al. This method has demonstrated good accuracy in predicting the erosion profile from the former studies but has not been applied to a radial pump. This function builds on the simplified version of the GLM function, outlined in Eq. (2) in sub-section 2.4, by adding the product of vapor fraction and pressure gradient. As a result, there are similarities between the two methods, the erosion areas predicted by these two functions yield similar projections when applied to a propeller [7].

Another erosion model developed by Fukaya et al. [30] known as the Direct Bubble Modelling (DBM), also shows very good accuracy with experimental data but is much more computationally expensive when compared to the other erosion models. DBM requires a separate model and involves modelling the growth and collapse of individual bubbles, which means very small time-steps and fine mesh is required when compared with the previous methods, so that the evolution of these individual particles can be resolved. This method has only been experimentally verified with a Francis turbine, which has a very different geometry compared to the subject pump and most commercial pumps. Due to the lack of experimental verification and significantly higher computational cost, this method is not selected on the current subject pump.

2.3 Erosion Mechanism

The erosion mechanism is explained in the following section using Figure 1 and Equations (2) to (9). The sequence of event starting from cavitation to erosion damage are summarized in the four key steps outlined in this section. Section 2.4 explains the equations related to the explained events during the cavitation process and subsequent erosion, then outlines how it is implemented in CFD. The diagram has been reproduced from the work of [6].

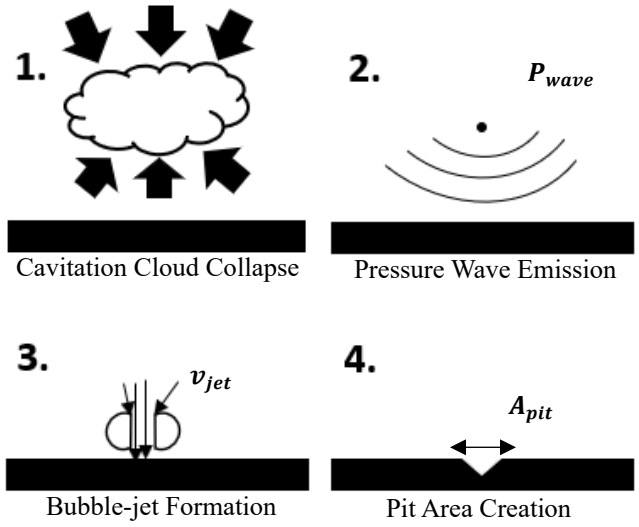

FIGURE 1: EVENTS RELATED TO CAVITATION DAMAGE

1. The cavitation cloud collapse creates a shockwave that spreads onto the fluid. The magnitude of the emitted pressure wave P_{wave} is closely related to the velocity of the change of the vapour cloud volume $(d\alpha/dt)$.
2. The magnitude of the shock wave as it travels towards the solid surface. The mathematical description that highlights events 1. and 2. have been summarised by Eq. (2).
3. Single bubbles are present near the solid surface. As the shock wave reaches the single bubbles near the surface, the bubbles begin to oscillate and form a bubble-jet with velocity v_{jet}, that damages the surface. Eq. (3) highlights the relationship governing the bubble jet creation. Eq. (4) and Eq. (5) outlines the criteria these jet bubbles must meet to induce erosion damage onto the surface. The minimum vapor fraction of $\alpha > 0.01$ is needed so that sufficient bubbles are present to cause erosion [31].
4. The high-velocity liquid jet from the bubbles v_{jet} impact the solid surface and erodes the surface creating a pit area A_{pit}. The magnitude of A_{pit} is directly related with the bubble-jet velocity v_{jet} as expressed by Eq. (4) to (9).

The main mechanism responsible for damage on the solid surface is from the water hammer stress that is generated by the velocity of the jet bubbles v_{jet}. The approach to predict erosion is based on when a threshold compressive stress is reached, and that after this point the deformation of the solid is fully plastic. The deformation, and thus pit area creation occurs only if the bubble jet velocity v_{jet} can result in a stress value that is high enough to overcome the yield stress of the material p_y, which is expressed by v_{crit}. As v_{jet} travels through the fluid, some of the energy is lost within the medium and some absorbed by the body of the material during impact. The excess energy that deforms the surface is highlighted by Eq. (5) velocity of deformation v_{def}. The excess energy from the impact expressed by v_{def} then creates the plastic deformation on the surface with pit area A_{pit}.

2.4 Implementation in CFD

The method by which the erosion damage is predicted in CFD is by utilizing field functions. All of the simulations are calculated using variables which have already been generated from the cavitation simulations and thus can be carried out with only a small addition to computational cost. The erosion algorithm is implemented in post-processing and is updated at the end of each time-step of the run.

The simplified Gray Level Method (GLM) works by taking the pressure observed at cell P with the vapor pressure P_v multiplied by the derivative of the vapour fraction α as highlighted by Eq. (2). A more rigorous implementation is highlighted by the subsequent Eq. (3) to (9) and is the focus of this work. The implementation has been verified with a hydrofoil in the works of Dular & Coutier-Degosha [32] and Peters et al [31], but never been implemented on a radial pump. Dular et al. did not use CFD to predict erosion in [6]. The CFD calibration simulations and comparison with experimental data can be found in sub-sections 4.1 and 4.2. In addition to being able to identify and quantify the erosion areas, this work is chosen as the radial pump used in the referenced work shares many characteristics with the subject pump, in that it has a similar blade geometry and operating characteristics. The sequence of calculations that have been used to implement the erosion model is outlined below:

$$P_{wave} = (P - P_v)\left(\frac{d\alpha}{dt}\right) \tag{2}$$

Eq. (2) highlights how the magnitude of emitted pressure wave P_{wave} is related to the velocity of the change of the vapour cloud volume from the cavitation cloud collapse. It is a simplified version of GLM implementation than can generate the approximate wear areas, and outlines the general principle of the more rigorous version of the erosion model. Eq. (2) can be implemented by itself without Eq. (3) to (9) to approximate the wear areas but this method will not be able to calculate the quantity of erosion damage.

$$v_{jet} = 8.97\gamma^2\sqrt{\frac{P - P_v}{\rho}} \tag{3}$$

v_{jet} is the jet velocity from bubble collapse that damages the metal surface, as portrayed by event 3 in Figure 1. As highlighted by equation 3, the magnitude of v_{jet} is dependent on the pressure of the surface and inversely proportional to the density. This implies that the erosion model implemented will over-predict the value of v_{jet} when there is large pressure advection, such as sharp LEs along the surface. Transition regions between vapor to liquid has lowest ρ and leads to higher estimated values for v_{jet}.

The observed pressure P and density ρ at the cell represents the combined values of the liquid and vapor mixture

in the medium. These variables are extracted from the CFD simulation at the end of each time-step to continuously update v_{jet} and subsequent equations to evaluate the erosion damage. P_v is the saturation pressure of the liquid valued at 3170 Pa. γ is the distance ratio from the center of the bubble to the surface of impact valued at 1.1, and 8.97 is a dimensionless constant. Both of these values are based on the experimental findings by Plesset and Chapman [33].

$$v_{crit} = \sqrt{\frac{p_y}{\rho}\left(1 - \left(1 + \frac{p_y}{B}\right)^{-1/n}\right)} \tag{4}$$

v_{crit} is the minimum velocity required for the jet bubble to deform the surface of the metal. p_y is the yield stress for the copper sensor used in the reference experiment and the constants *n* and *B* are outlined by the experimental work of Lush [34]. The values used in the simulations are 200 Mpa, 300 Mpa, and 7 (dimensionless) for each of those respective variables. v_{crit} in this case 118.5 m/s, any excess velocity from this value is converted to damage the surface. The vapor fraction must also be x > 0.01 on the surface, so that there are significant enough number of bubbles present to cause erosion [31].

$$v_{def} = v_{jet} - v_{crit} \tag{5}$$

v_{def} is the excess energy from v_{crit} that quantifies the magnitude of damage to the impeller surface. As a condition, $v_{jet} > v_{crit}$ so that plastic deformation can occur and cause harmful damage to the surface. The excess energy v_{def} represents the magnitude of energy that causes damage on the solid surface. A key assumption of this equation is that the treatment of the surface is fully plastic once this threshold velocity value v_{crit} is met, and therefore all the excess kinetic energy from bubble jet v_{def} is used to deform the surface of the blade.

$$t_{def} = \frac{r_{jet}}{c_l} \tag{6}$$

t_{def} is the time required for the bubble jet to travel across its radius of travel r_{jet}, while c_l is the bubble sonic velocity. The value of this assumed to fixed on the implementation of this model. Their respective values are set at 10μm and 1484 m/s based on the experimental work of Plesset and Chapman [33].

$$d_{pit} = v_{def} t_{def} \tag{7}$$

d_{pit} is the pit surface diameter from the subsequent bubble jet collapse, which is a product of the deformation velocity v_{def} and the transit time of the bubble jet t_{def} across the surface of the solid body. Since t_{def} is a fixed value from experimental data, the d_{pit} is directly proportional to v_{def}, which in turn is directly related to v_{jet}. Since v_{jet} is directly proportional to pressure and inversely proportional to the density of the fluid mixture, the erosion model proposed predicts the peak of the erosion values where the pressure gradient is highest. The value of vapour fraction across the area determines the likelihood of erosion.

$$A_{pit} = \pi\left(26.7 d_{pit}\right)^2 \tag{8}$$

A_{pit} is the pit area calculated from the pit diameter d_{pit} and the coefficient 26.7 is based on the experimental results from Fortes-Patella et al [35].

$$A_{dam} = \frac{\sum_{t_{start}}^{t_{end}} A_{pit}}{A_{ref}} . \frac{T}{\Delta t} \tag{9}$$

A_{dam} quantifies the relative erosion damage on the impeller surface, where A_{ref} is the referenced area of the blade in question. T is incubation time from experiments and Δt is the time between each timestep within simulation. This second term provides the scaling factor to scale-up the smaller values of A_{pit} from the shorter simulation time so that it is comparable with experimental data. The experimental data represents the sum of the erosion damage from one hour of cavitation. This approximation is acceptable as erosion wear is linear over time [20, 32, 36]. t_{start} and t_{end} represent the time of start and end of the sampling interval for the summation of the erosion damage area. t_{start} is chosen at the end of the pressure transient in the beginning of simulation and t_{end} the value at the end of the 38ms sampling interval. This time interval is chosen as this value is the interval suggested by the authors in the referenced work [32].

Above is the abridged version of the calculation of the area of damage A_{dam} starting from the calculation of v_{jet}, which uses variables extracted from CFD. More details on the origins of the equation terms and definition of the constants used can be found in Dular et al [6, 32, 37, 36] as well as Plesset and Chapman [33].

Although this method has demonstrated some agreement with experimental data as highlighted by the results in section 4, a fundamental drawback of the method is that it assumes that the bubble jet, vapor and subsequently the creation of the pitting areas are in the same location, and that this holds true under all cavitating conditions. In reality, the bubbles may differ as they travel across the fluid. and may displace some distance in the horizontal direction before colliding onto the surface. The erosion model does not take this into account, which is a contributing factor in the disagreement with experimental data.

3. METHODOLOGY

The CFD simulations carried out attempts to provide insight to how cavitation erosion would occur on a two-stage pump, how its rotation speed could influence the affected areas. Cavitation is stimulated by lowering the pressure observed at the pump inlet. The areas which have most significant vapor build-up as a result of cavitation can be identified by monitoring the vapor fraction scalar field, but the areas most affected by erosion effect

are identified by implementing GLM. A detailed breakdown of how this erosion model works is described in sub-section 2.1.

A two-stage pump is chosen as the subject pump for the simulations carried out. The pump is powered with an AC motor and is designed to operate at either 2900 RPM or 3500 RPM. Both impellers have the same blade geometry with a static diffuser in between the two stages to reduce turbulent flow and improve efficiency. This pump is chosen as its geometry, fluid-mechanic performance and operation is representative to many commercial multi-stage pumps used across different industries, so that the findings from this work are applicable to a wide range of pumps.

The simulations are carried out using commercial CFD software Star-CCM+ [38]. The subject pump used for the erosion experiment is 3D scanned so that its geometry is accurately represented in the digital domain and a representative CFD simulation of the pump could be run. Star-CCM+ is chosen to run these cavitation simulations for several reasons: the software can resolve unsteady rotor and stator interactions, has the required turbulence and cavitation models, and stable compatibility with 3D scanning file formats [1, 21].

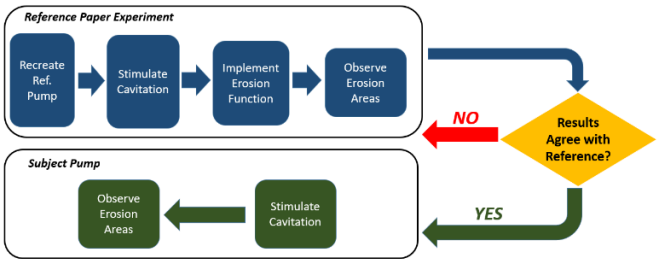

FIGURE 2: SEQUENCE OF STEPS TO PREDICT EROSION USING CFD AND APPLICATION TO SUBJECT PUMP

Figure 2 summarizes the sequence of simulations carried out in this work: First, the pump and hydrofoil used in the reference work by Dular et al. [6] is re-created with CFturbo using the specifications outlined in the paper. The primary goal of the hydrofoil simulation is to verify the basic functionality of the GLM algorithm, by means of testing with a simple geometry. A fully detailed instruction on how to couple the GLM erosion model with CFD simulation can be found in the reference work by Dular & Coutier-Degosha [32]. Cavitation is stimulated with the same boundary conditions outlined in the reference work to calibrate the results. Once successful calibration and validation has been achieved with the simulation, the GLM function is applied to the subject pump with the same boundary conditions as the reference pump. The work carried out by Dular et al [6] is chosen as the field function described has shown strong agreement with the experimental results, using a test pump that has a similar impeller geometry as the subject pump.

3.1 General Configuration for all Simulations

All the CFD simulations carried out in this work in Star-CCM+ share many common features in their configuration with each other. All simulations are performed as multiphase calculations with water and water vapor used as the liquid and gas model respectively with initial parameters at 20°C, using a constant density fluid model, with a Saturation pressure P_{sat} of 3170 Pa. This yields a liquid/vapour density ρ_l and ρ_V of 998.2 kg/m^3 and 0.5953 kg/m^3 respectively. Prior to the results discussed in Section 4, the cavitation models were compared with the reference pump and hydrofoil simulations to see which had better agreement with experimental data from [6, 32]. The Scherr-Sauer cavitation model [39] has been chosen over the Rayleigh-Plesset model [40] as it has been shown to follow the reference experimental data more closely. Likewise, the κ-ω SST turbulence model has been chosen over κ-ε as the former shows closer agreement with experimental data. The selection of both cavitation and turbulence has been narrowed down based on a literature survey of previous works for cavitation [1, 2, 3, 4, 5]. The bubble density N_b and radius R_b has been set to $5\text{x}10^8$ and $1\text{x}10^{-5}$ based on suggestions by Peters et al. [31]. All simulations use implicit unsteady, segregated fluid and Volume of Fluid models with a second-order solver.

The primary difference between the simulations is the geometry, mesh set-up and simulation time with each timestep Δt. Mesh density is increased significantly near and on the blade surfaces for all simulations, as this is the area that is most affected by erosion. All the simulations reference an incubation time of 3600 seconds to project the erosion wear from one hour of cavitation. The sum of erosion damage is sampled over a time period of 38 ms, and scaled to be equivalent to one hour of running as suggested by the reference work [32]. Since the wear progression increases almost linearly over-time, this method of projection is deemed to be acceptable and still showed close agreement with experimental data [6].

3.2 Reference Hydrofoil Configuration

The first simulation is carried out on a 2D symmetrical hydrofoil inside a rectangular box. The primary aim of these simulation is to verify the basic functionality of the erosion model being applied.

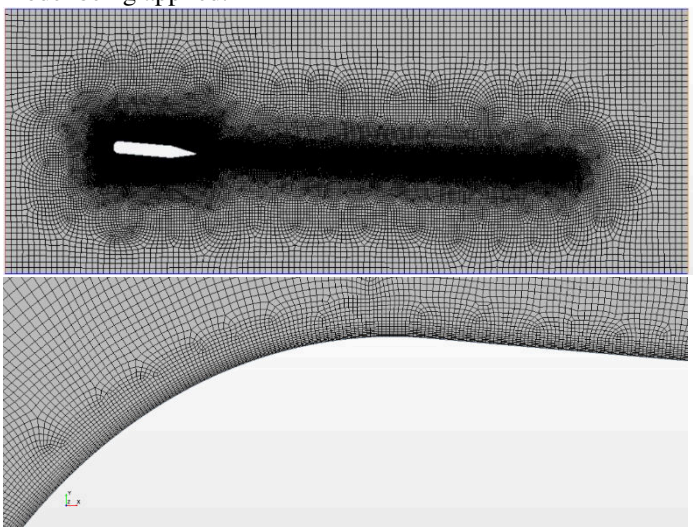

FIGURE 3: MESH STRUCTURE OF THE REFERENCE HYDROFOIL (TOP) AND CLOSE UP (BOTTOM)

A quadrilateral mesh is used in consisting of approximately 359k cells. A timestep of Δt = 8.3E-6 is chosen as this is 1/1000th of the transit time for the fluid passing through the tunnel. A velocity inlet and pressure outlet are used for the rectangular box containing the hydrofoil. Figure 3 shows the general set-up of the hydrofoil simulation in the 2D plane, with a zoom-in of the mesh at the transition area between the blunt leading edge (LE) and flat surface.

3.3 Reference Pump Configuration

Before the erosion algorithm could be implemented, the results must first be calibrated so that the erosion algorithm is consistent with the experimental data. The reference pump is re-created in CFturbo based on the specifications outlined by Dular et al. [6] and Bachert et al. [41]. The reference pump shares many similar characteristics with the subject pump in that it is designed to operate a similar specific speed, has 5 blades with similar blade angles. The primary difference is that the reference pump is wider and is a single-stage pump. Because of these similarities, the erosion algorithm verified on the reference pump can be applied to the subject pump. The reference pump is created using a large, symmetric case so that the wear distribution among the blades is more uniform.

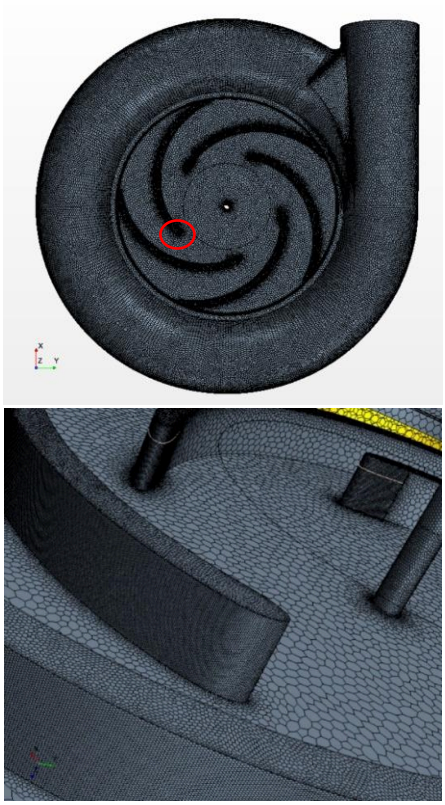

FIGURE 4: MESH STRUCTURE OF THE REFERENCE PUMP (TOP) AND CLOSE UP OF THE BLADE MESH (BOTTOM)

Figure 4 shows the general set-up of the reference simulation in 3D when viewed from the top, with a zoom-in of the mesh at one of the pump blades LE on the bottom screenshot. The rectangular enclosure and the top shroud of the pump case is not shown in figure 5.

A mass outlet is used at the pump outlet and a stagnation inlet is used at the pump inlet so that the flow at the outlet and suction head at the pump inlet can be varied. The pump is contained inside a rectangular box to improve the flow continuity of the model. A polyhedral mesh is used with 3.2M cells globally and with 2.4M on the blade. A timestep of Δt = 3.35E-5 is chosen as this results in 0.5 degree of the impeller rotation per timestep.

3.4 Subject Pump Configuration

The 3D scanned pump is imported to Star-CCM+ as a .STL file. Surface wrapping is carried out so that any surface anomalies on the 3D geometry are corrected. Figure 5 shows the mesh set-up of the subject pump at various viewing angles.

FIGURE 5: MESH STRUCTURE OF THE SUBJECT PUMP

Figure 5 (top) shows a cut-away representation of the pump mesh, with the impeller made visible. The rectangular box containing the pump is not shown in the picture, which serves to improve flow continuity of the model. Figure 5 (middle) represents the impeller blade when viewed from the top and Figure 5 (bottom) is a close-up view of the blade mesh. As highlighted by these figures, the blade is largely straight at the LE and at a steep curvature section there is a steep increase in the blade angle. The pump inlet is seen on the top pipe connection, and the outlet is the pipe length protruding on the side of the pump. The first impeller on the top interfaces with the incoming fluid and provides the initial boost. The second impeller boosts the pressure output into greater levels and interfaces with the pump outlet. A short pipe is created at the inlet and a long pipe section is used to simulate the pipe connection to the rest of the system and to reduce the effects of backflow.

A polyhedral mesh is used in consisting of approximately 11M cells. A timestep of Δt = 4.72E-5 is chosen when the pump is running at 3500 RPM and a timestep of Δt = 5.75E-5 is chosen when the pump is running at 2900 RPM as both of these constitute 1.0 degree per timestep. It was found that these timesteps provided adequate level of resolution but allowed reaching convergence in a timely manner to compensate for the relatively high cell count. The pump flowrate is fixed at 0.83kg/s as this represents approximately 55% of the maximum pump flowrate, which is a typical operating point of the pump.

Prior to running the cavitation simulations, the pump performance is calibrated for operation under non-cavitating conditions to ensure that the simulated model is representative to how the pump would perform in reality. The pump is validated against the manufacturer datasheet and the pump performs as according to the manual with an error of 3%, which is within the uncertainty of the manufacturer measurements.

3.5 Grid Sensitivity Analysis and Accuracy of Numerical Solution

The set-up for the reference pump outlined in section is the subject of the grid convergence study, as it allowed the numerical solution to be compared directly with experimental data. The focus of the grid convergence study had been done on refining the mesh on the blade surface of the pump, as this was found to have had the most influence on the accuracy of results. The values used in the study is the sum of A_{dam} over the sample interval of the damage calculation. The methodology for the grid convergence study follows the article by Celik [42] in ASME Journal of Fluids. The basic definitions related to grid study and related equations can be found in this work.

The boundary conditions chosen is from case B for the reference single stage pump when cavitation number σ = 0.275, Q = 99.4%. The reference pump is chosen at this boundary condition as from the results from section 4.2.

The mesh size on the blade surface for coarse, moderate and fine meshes are 1.15E6, 2.4E6 and 4.4E6 cells. Those respective meshes have normalized residuals (continuity) in the order of 5E-4, 3E-4 and 1.5E-4. Grid refinement factor of 1.67 and 1.5 has been used between moderate & fine and coarse & moderate meshes respectively.

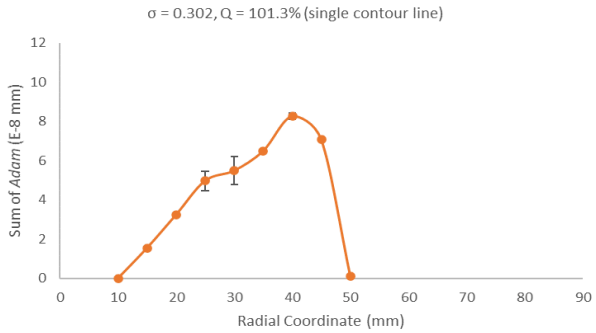

FIGURE 6: EXTRAPOLATED VALUE FROM THREE MESHES

Figure 6 shows the extrapolated value from the three meshes for a single contour line on the blade center. This allows the degree of numerical accuracy to be understood for each curve on the blade. The global order of accuracy for the numerical solution is p_{ave} = 2.2, with values ranging from 0.01 to 5.69 for local order of accuracy p. Numerical uncertainty according to the Grid Convergence Index (GCI) is 4.08% on average, with a maximum discretization uncertainty of 13.27%, valued at ± 6.6E-9 mm on x = 30. The primary regions which exhibit the largest uncertainty are at x = 25mm and x = 30mm, where oscillatory convergence is also observed. The other 7 out of 9 points observed monotonic convergence. Refinements can be made to reduce the discretization uncertainty at the two points but at a significant increase to computational cost.

4. RESULTS AND DISCUSSION

Below are the results from the CFD simulations when compared with the reference experiment from [6, 32]. The application of the erosion algorithm of the subject pump is investigated at two pump speeds: 2900 RPM and 3500 RPM to understand the effects of rotational speed to the rate of erosion.

4.1 Reference Hydrofoil

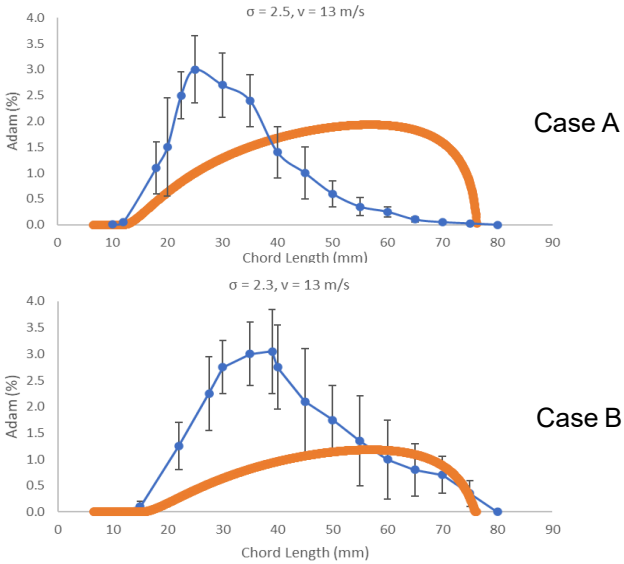

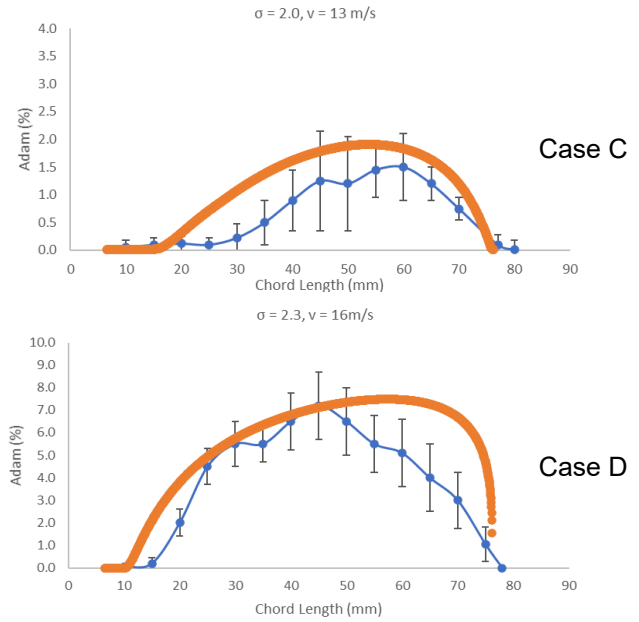

FIGURE 7: WEAR DISTRIBUTION ACROSS REF. HYDROFOIL

Figure 7 represents the result from the hydrofoil simulations. The experiments have been given designation from case A to case D. The blue lines represent experimental data from the reference work and the orange lines represent the output from CFD simulations. The x-axis represents the chord length of the hydrofoil in the x-axis, starting at x = 0mm at the LE and x = 85mm at the end of the flat surface. The y-axis represents the relative damage area of the hydrofoil. Across the entire length of the hydrofoil, vapor fraction, $\alpha > 0.01$, hence the erosion value will be strongly dependent on the value of pressure P, as there is significant number of bubbles already present on the surface. As a result of this, there is over-estimation on the erosion values on points of the surface where pressure is highest. This highlights a weakness of GLM for use on hydrofoils, but the model is still able to predict the erosion depth at similar values to the experimental data, with the primary error is mainly where the peak maxima of where the damage is estimated.

As highlighted by cases C and D, the CFD shows some agreement with experimental data, within the error bars for some of the measurement points. Cases A and B show the least amount of agreement with experimental data. The wear distribution estimated by case A has a similar envelope with the experimental data but estimates the peak value at a different location along the chord length. The disagreement for Case B shows the disagreement in values is observed at the LE to the midpoint of the hydrofoil. Better agreement with experimental data is achieved as chord length is moved to the trailing edge, shown that the simulation points are able to predict within the error bars. For all cases, the erosion algorithm estimates the highest quantity of wear at approximately the same location at x = 60mm along the chord of the hydrofoil, which is where the pressure gradient is the highest. This point is part of the transition between the flat surface to the slope of the hydrofoil. The primary weakness of the algorithm is that it that the jet velocity v_{jet} and thus the pit area A_{pit} is directly proportionate to the square root of the pressure at that cell P. The implementation of the algorithm by the referenced authors [6, 32, 31] also shows similar results, in that the peak erosion values are concentrated on a single point along the surface.

Furthermore, for this 2D case, the results are only from a single contour line across the chord length, whereas on the pump it is from multiple curves across the blade thickness. This creates an averaging affect where some points along the curve, on the different the thicknesses experience less erosion. This leads to a better agreement with the experimental results. For the hydrofoil, In-spite of its inability to replicate the erosion profile from the experimental data, it is still able to quantify the approximate width and depth of damage.

4.2 Reference Pump

Figure 8 is a 3D visualization of the iso-surface for the suction side of the impeller blade, whereas Figure 9 is the 2D graphical representation for the same component.

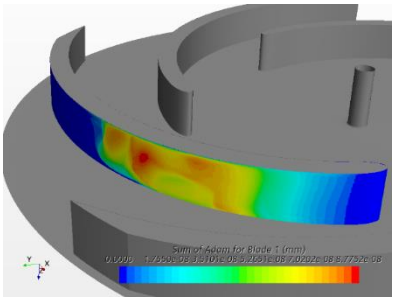

FIGURE 8: ISO-SURFACE OF EROSION-SENSITIVE AREAS ON REFERENCE PUMP IMPELLER FOR CASE C

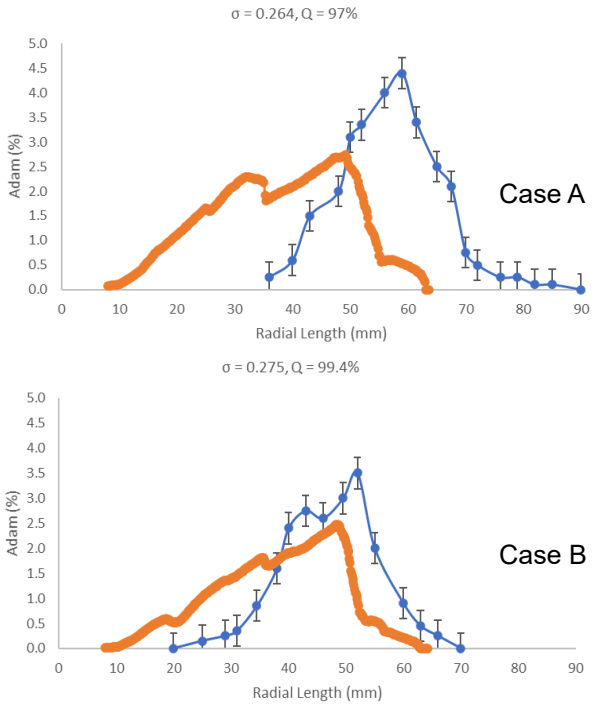

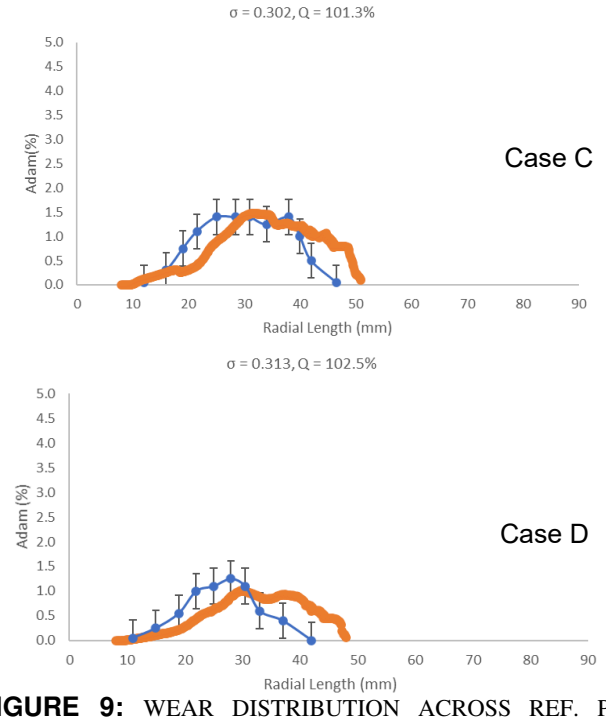

FIGURE 9: WEAR DISTRIBUTION ACROSS REF. PUMP

Like the hydrofoil, the simulation results in Figure 9 have been given designation from case A to case D, starting from the top to bottom. The x-axis represents the radial coordinates of the pump blade, starting at x = 0mm at the blade LE and x = 90mm at the TE of the blade. The y-axis represents the relative damage area of the impeller. The damage profile on the blade represents the average value of erosion area across the thickness of the blade in each of the radial coordinates. For each coordinate, the erosion damage area is added up across the blade thickness and is divided by it so that a 2D visualization can be made and compared with experimental data. Figure 8 is a 3D visualization of the boundary conditions represented by case C.

Case A shows the largest disagreement with experimental data. In spite of this, the approximate width and depth is similar to experimental data but shifted 25mm along the radial coordinates. The primary disagreement comes from a shift of the peak value of the erosion. This due to the sheet cavitation separation near the LE, at x = 30mm and the collapse of the vapor cloud at x = 60mm. The erosion model estimates erosion on areas which are directly underneath the vapor sheet and does not take into how bubbles deviate as a result of the cloud separation.

Cases C and D shows closest agreement with experimental data with more than half of the data points being within the experimental error bar. Case B overestimates the wear at the blade LE and underestimates at the TE, shown by the shift in coordinates by 10mm. Cases C and D has a similar shift in the wear estimation by 5mm. Cases D and C have much lower wear because $v_{jet} < v_{crit}$ at x > 50mm, hance no erosion predicted. This is due to the lower severity of cavitation that resulted in lower pressure waves at these areas.

The radial coordinates x = 10mm to 60mm have $\alpha > 0.01$. Hence in this region erosion value will be strongly dependent on the value of pressure P, as there are a significant number of bubbles present on the surface. For cases A and B, the model predicts that transition erosion is greatest at $x = 49$, where α drops by 0.2. This area in addition to being a pressure peak is also a region where a significant portion of the vapors transition back into liquid, decreasing the value of density ρ. As highlighted by eq (2). This contributes to an increased value of v_{jet} and subsequently A_{pit} for this region of the blade.

The model also assumes that the bubbles erode on the same location as the vapor cloud and hence this leads to a major shift in the center of maxima of the predicted erosion. It does not consider the erosion affected by cavitation cloud separation. Further improvements to the model would be to adjust the erosion predictions to take into account how the bubbles travel under different cavitating conditions.

4.3 Subject Pump – 2900 RPM

The results from this simulation highlight the result of the erosion algorithm when applied to the subject pump and rotating at 2900 RPM.

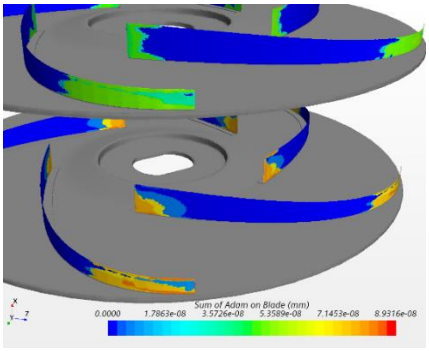

FIGURE 10: ISO-SURFACE OF EROSION-SENSITIVE AREAS.

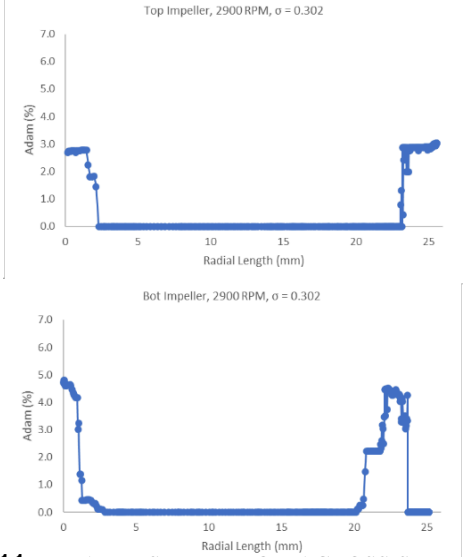

FIGURE 11: WEAR DISTRIBUTION ACROSS SUBJECT PUMP AT 2900 RPM

Figure 10 is the 3D iso-surface of the erosion areas whereas Figure 11 is the 2D representation of Figure 10 for the first (top) and second stage (bottom) impellers respectively.

This increased erosion wear at the blade LE and TE is due to the higher-pressure gradient at these points, where vapor fraction, $\alpha > 0.01$. The cause of the sharp pressure gradient at the blade LE ($x = 0$) is due to the squared shape of the blade, whereas in the reference pump, near the blade LE ($x > 22$mm) has a steep blade angle. The erosion areas are the highest when the blade curvature is steepest, as this is where the pressure gradient is likely to be the largest hence v_{jet} and subsequently A_{pit}.

For the first stage, vapor $\alpha > 0.01$ across entire surface area of the impeller, but for 2900 RPM case there is insufficient pressure for v_{jet} to exceed v_{crit} of 118.5 m/s. For the second stage impeller, $\alpha > 0.01$ is present at concentrated regions at $x =$ 22mm and $x = 0$, the blade LE and curvature. This combined with the much higher pressure on the second stage of the impeller permits in higher jet velocities v_{jet} that results in wear.

4.4 Subject Pump – 3500 RPM

The results from this simulation highlight the result of the erosion algorithm when applied to the subject pump when rotating at 3500 RPM. Apart from the difference in rotation speed, the boundary conditions are identical to that of the 2900 RPM case.

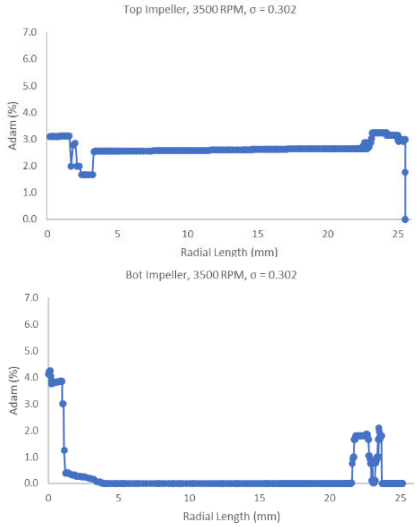

FIGURE 12: WEAR DISTRIBUTION ACROSS SUBJECT PUMP AT 3500 RPM

Figure 12 is the 2D representation of the damage areas for the first and second stage impeller of the pump. For the first stage, $\alpha > 0.01$ across the entire surface area of the impeller, but for the 3500 RPM case there is sufficient pressure P for v_{jet} to exceed v_{crit} of 118.5 m/s. The higher overall pressure from the 3500 RPM case generates enough pressure that would produce a high enough v_{jet} to cause damage to the surface. Like the 2900 RPM case, the second stage impeller, $\alpha > 0.01$ is present at concentrated regions at $x =$ 22mm and $x = 0$, at the blade LE and peak curvature. Due to the much higher pressures of the second stage, the pressure waves are more severe resulting in a much more severe erosion at those specific areas.

As highlighted by the two RPM cases, the pressure of the cavitation shockwave P influences severity of erosion, whereas the fraction of vapor α in the area dictates the likelihood of erosion. If $\alpha < 0.01$ erosion will not take place as there is insufficient concentration of bubbles, but if P is too low, v_{jet} cannot exceed v_{crit} to damage the surface.

4.5 Summary of Results

The boundary condition with the least agreement, such as Cases A for the single-stage pump showed a shift in start, peak and end of the erosion sensitive areas but the erosion depth and width are of similar values. Cases B, C, and D shows the best agreement with the experimental data, as their envelope is well-aligned with experimental data, but with a shift of 10mm for case B and 5mm for cases C & D in the radial coordinates. The disagreement with Case A is due to the sheet cavitation separation near the LE, at $x =$ 30mm and the collapse of the vapor cloud at $x =$ 60mm. The erosion model does not take this into account and hence has leads to a shift in the predicted values.

The erosion model struggles to predict the exact areas of the 2D hydrofoil that is most susceptible to erosion and is biased at approximately $x =$ 60mm, as this is the point of the hydrofoil that shows a transition from the flat surface and to the slope at the TE. This sharp surface contributes to a sharp increase of P measured on the surface and thus over estimates of v_{jet} and subsequently A_{pit}. In-spite of this, the width and depth of the predicted areas are within the same ball-park values.

The erosion model showed better agreement with the radial pump than hydrofoil, as highlighted by cases B, D and C. In these conditions the profile of the erosion was similar but with a shift of 10mm for case B and a shift of 5mm for cases C and D on the radial coordinates. Case A showed least agreement but the approximate width and depth of erosion was similar to experimental data. A source of discrepancy between experimental and simulation is the slightly different volute design, which also contributed to the disagreement with experimental data. The volute was not replicated exactly due to the authors not disclosing the exact dimensions in [6, 41].

For the reference pump the curvature of the blade angle peaked at approximately $x =$ 49mm whereas for the subject pump the blade curvature peaked at $x =$ 22mm and $x =$ 0mm due to the sharp, squared edge. At both of these radial coordinates it was also found that the erosion wear was most severe. These sharp peaks and curves not only produce a concentration of high pressure but also sufficiently high vapor to produce erosion.

For the two-stage pump, the first-stage impeller (top) is likely to see a lower value of erosion at a single point but is spread more evenly, whereas the second-stage impeller (bottom) observes greater erosion at concentrated areas. In order to produce harmful erosion, not only does it need to be sufficient amount of pressure, but there needs to be sufficient vapor so that the bubbles could be generated.

The user must consider points on the surface where there will be peak values in pressure as these are the points where large value of P is observed and the algorithm over-estimates v_{jet} and hence A_{pit}. The distribution of α must also be understood as that also influences the distribution of erosion.

5. CONCLUSION

This work has demonstrated how to implement the GLM function to predict cavitation erosion on a hydrofoil and radial pump by using a commercial CFD package. It is the first time the full GLM algorithm is implemented on a radial pump using commercial CFD software. The erosion prediction algorithm is also implemented for a two-stage pump for the first time. In spite of the flaws in the accuracy of predictions in simulations, the results are still useful for pump designers and operators. The key findings, suggested future work and benefits are summarized in the following sub-sections.

5.1 Key Findings

- **Suitability for Pumps:** It was found that GLM was more accurate in predicting the erosion sensitive areas on a radial pump compared with a hydrofoil. For a hydrofoil, the model over-estimates the erosion wear and incorrectly predicts it to be on a single coordinate for all boundary conditions. For the pump, the simulations were still able to predict the approximate severity of the erosion across the surface, in spite of slight shifts in radial coordinate for the predicted damage.
- **Compatibility with Commercial CFD**: Previous implementations of the erosion model have been carried out with open-source CFD packages, which are less easy to implement. Previous implementation of GLM with commercial CFD software by authors [7, 28] used a simplified model by using Eq. (2) only. This version is able to highlight the areas vulnerable to erosion but does not show the magnitude of volume loss and is less accurate. GLM on radial pump by Dular et al. [6] did not use CFD.
- **Dependency on Impeller**: For a pump, the erosion areas are dependent on the impeller design, specifically in areas with steep curves or sharp angles where there is a large gradient in pressure. The model predicts the peak erosion damage at approximately the same areas on the blade surface. This is due to the inherent weakness of the algorithm as stated in Eq (3) where v_{jet} and hence A_{pit} is directly proportional to the pressure value on the blade surface.
- **Dependency on Pump Case**: Another source of disagreement between the simulation and experimental data was from the pump geometry. The pump used in simulations are not exactly the same as the geometry used by the experimental work [6, 41]. Limited information was shared by the author related to the experimental pump casing. The experimental pump had a unique design which had 12 outlets underneath the volute and its design is very difficult to replicate. In spite of the differences from the pump volute, the simulations were still able to predict the erosion areas well aligned with the reference experiment. This highlights that the case design of the pump contributes less significantly to determining where the erosion areas are concentrated.
- **Bubble Displacement**: For different cases of cavitation, the bubbles may travel a distance of a few millimeters along the blade before collapsing on to the surface of the pump, hence the experimental data shows that there is a shift in the value at which peak erosion lies. The erosion model implemented does not take into account the different cavitation conditions and differences in bubble collapse. It applies the same equation for all cavitating conditions, which is one of the weaknesses of using the model.

5.2 Future Work

- **Further Testing of GLM**: The research demonstrated in this paper can be improved by further testing of GLM using different pump designs. The extent at which the pump volute influences the erosion areas could be better understood. Further testing of GLM with different blade geometries can also be beneficial to understand how well it estimates erosion. Additional experimental data would need to be generated to support the findings from these studies, as at the moment experimental data only exists for hydrofoils, single-stage radial pumps and propellers.
- **Comparison with other Erosion Models**: A feasibility study can also be done to examine which applications of GLM excels and further investigate its accuracy and limitations. Comparison of different erosion algorithm erosion models with the geometry used in the paper such as DBM, IFM and EPM methods can be done to examine its accuracy when compared with experimental data.
- **Improvement to Estimation of A_{pit}:** The erosion algorithm assumes that v_{jet} behaves uniformly for all cavitating conditions, when in reality the different severities of cavitation influence the mechanism that the bubble travels and collapses on the surface. An improvement can be made to the erosion model where some conditional modifier exists for v_{jet} to adjust according to the cavitation severity. This correction factor would adjust for how the bubble travels at different cavitation conditions.

5.3 Benefits of Research

In spite of some disagreement with experimental data on certain boundary conditions, the erosion model is able to estimate the depth and width of the damage areas. GLM is practical as it uses field variables already computed by the cavitation simulation. The results can be used as part of accelerated fault testing to create some form of condition monitoring solution. Pump designers could significantly decrease the duration of the design process in testing for cavitation resistance by having the erosion model predict the potential damage areas. The ability to predict long-term cavitation erosion in the early stage of the design allows more opportunities to optimise the blade design and mitigate erosion.

The erosion model can be generally improved by taking into consideration different cavitation mechanisms, which as highlighted by the data, was one of the sources of discrepancy between the experimental data and simulation data.

ACKNOWLEDGEMENTS

This research is funded by United Kingdom Research and Innovation (UKRI) formerly known as the Engineering Physical Sciences Research Council (EPSRC).

REFERENCES

[1] E. Bennett, "CFD Analysis of Unsteady Cavitation Instabilities in a Turbopump," in *ISimT-16 Symposium on Innovative Simulations in Turbomachinery*, 2016.

[2] M. Sedlar, S. Oldrich and M. Komarek, "CFD Analysis of Cavitation Phenomena in Mixed-Flow Pump," *International Journal of Fluid Machinery and Systems,* vol. 5, no. 1, pp. 18-29, 2012.

[3] M. Sedlar, P. Zima, M. Bajorek and T. Kratky, "CFD Analysis of Unsteady Cavitation Phenomena in Multistage Pump with Inducer," in *IOP Conference Series: Earch and Environmental Science, 2012*, 2012.

[4] F. C. Visser, R. J. H. Dijers and J. G. H. op de Woerd, "Numerical Flow-Field Analysis and Design Optimisation of a High-Energy First-Stage Centrifugal Pump Impeller," *Computing and Visualisation in Science,* vol. 3, pp. 103-108, 2000.

[5] L. D'Agostino, "Turbomachinery Developments in Cavitation," Nato, Pisa, 2011.

[6] M. Dular, B. Stoffel and B. Sirok, "Development of a Cavitation Erosion Model," *Journal of Wear,* vol. 261, p. 642–655, 2006.

[7] O. Usta, B. Aktas, M. Maasch, T. Osman, M. Atlar and E. Korekut, "A study on the numerical prediction of cavitation erosion for propellers," in *Symposium of Marine Propulsion (SMP'17)*, Finland, 2017.

[8] T. Li and T. Van Terswiga, "On the capability of a RANS Method to Asses Cavitation Erosion on a Hydrofoil," in *Proc. of 8th International Symposium on Cavitation*, Singapore, 2012.

[9] J. Messina, P. Cooper and C. Heald, Pump Handbook, McGraw-Hill Publishing, 2008.

[10] M. Richings, The Prediction of Cavitation in High Speed Centrifugal Pumps, Durban: University of KwaZulu-Natal, 2014.

[11] R. Balasubramanian, E. Sabini and S. Bradshaw, "Influence Of Impeller Leading Edge Profiles On Cavitation And Suction Performance," in *Proceedings of the Second Middle East Turbomachinery Symposium*, Doha, 2012.

[12] S. L. Dixon and C. A. Hall, Fluid Mechanics and Thermodynamics in Turbomachinery, Amsterdam: Elsevier, 2010.

[13] G. R. Addie and A. Sellgren, "The Effect of Wear on the Performance of Centrifugal Slurry Pumps," in *Proceedings of ASME Fluids Engineering Division Summer Meeting*, Washington, 1998.

[14] S. Bross and G. Addie, "Prediction of Impeller Nose Wear Behaviour in Centrifugal Slurry Pumps," *Experimental Thermal and Fluid Science,* vol. 26, pp. 841-849, 2002.

[15] M. A. Rayan and M. Shawky, "Evaluation of Wear in a Centrifugal Slurry Pump," in *Proceedings of the Institution of Mechanical Engineers. Part A, Journal of Power and Energy*, 1989.

[16] C. I. Walker, "Slurry Pump Side-Liner Wear: Comparison of Some Laboratory and Field Results," *Wear,* vol. 250, pp. 81-87, 2001.

[17] C. I. Walker and A. Roudnev, "Slurry Pump Impeller Wear: Comparison of Some Laboratory and Field Results," in *Proceedings of the 15th International Conference of Hydrotransport*, Banff, 2002.

[18] H. Xu, W. Chen and C. Xu, "Cavitation Performance of Multistage Slurry Pump in Deep-Sea Mining," *AIP Advances: Fluid and Plasmas Collection,* vol. 9, pp. 1-17, 2019.

[19] A. Adamkowski, A. Henke and M. Lewandowski, "Resonance of torsional vibrations of centrifugal pump shafts due to cavitation erosion on impeller,"

Engineering Failure Analyses, vol. 70, pp. 56-72, 2016.

[20] M. Ylonen, Cavitation Erosion Characterization of Francis Turbine Runner Blade Material, Tampere: Tampere University of Technology, 2016.

[21] E. Bennett, "Cavitation CFD using STAR-CCM+ of an Axial Flow Pump with Comparison to Experimental Data," in *Star Global Conference 2014*, Vienna, 2014.

[22] J. Zhu and H. Zhang, "Numerical Study on Electrical Submersible Pump Two-Phase Performance and Bubble Size Modelling," University of Tulsa, Tulsa, 2017.

[23] M. Hundsagen, M. Mansour, D. Thevenin and R. Skoda, "Numerical Investigation of Two-Phase Air-Water a Centrifugal Pump with Closed or Semi-Open Impeller," in *Proceedings of 13th European Conference on Turbomachinery Fluid Dynamics & Thermodynamics* , Lausanne , 2019.

[24] N. Hasuike, S. Yamasaki and J. Ando, "Numerical Study on Cavitation Erosion Risk Of Marine Propellers," in *Proceedings of the 7th International Symposium on Cavitation*, Michigan, 2009.

[25] M. Nohmi, T. Ikohagi and Y. Iga, "Numerical Prediction Method of Cavitation Erosion," in *ASME 2008 Fluids Engineering Division Summer Meeting collocated with the Heat Transfer, Energy Sustainability, and 3rd Energy Nanotechnology Conferences* , Florida, 2008.

[26] S. Schmidt, I. Sezal, G. Schnerr and M. Thalmer, "Numerical Analysis of Shock Dynamics for Detection of Erosion Sensitive Areas in Complex 3-D Flows," in *Cavitation: Turbo-machinery & Medical Applications*, Warwick, 2008.

[27] A. Boorsma and S. Whitworth, "Understanding Details of Cavitation," in *Second International Symposium on Marine Propulsors*, Hamburg, 2011.

[28] C. Eskilsson and R. Bensow, "Estimation of Cavitation Erosion Intensity Using CFD: Numerical Comparison of Three Different Methods," in *Fourth International Symposium on Marine Propulsors*, June, 2015.

[29] C. S. Koksal, O. Usta, B. Aktas, M. Atlar and E. Korkut, "Numerical Prediction of Cavitation Erosion to Investigate the Effect of Wake," *Journal of Ocean Engineering,* vol. 239, pp. 1-19, 2021.

[30] M. Fukaya, Y. Tamura and Y. Matsumoto, "Prediction of Cavitation Intensity and Erosion Area in Centrifugal Pump by Using Cavitating Flow Simulation with Bubble Flow Model," *Journal of Fluid Science and Technology,* vol. 5, no. 2, pp. 305-316, 2010.

[31] A. Peters, H. Sagar, U. Lantermann and O. Moctar, "Numerical Modelling and Prediction of Cavitation Erosion," *Wear,* Vols. 338-339, pp. 189-201, 2015.

[32] M. Dular and O. Coutier-Degosha, "Numerical Modelling of Cavitation Erosion," *International Journal for Numerical Methods in Fluids,* vol. 61, pp. 1388-1410, 2009.

[33] M. Plesset and R. Chapman, "Collapse of an Initially Spherical Vapour Cavity in The Neighbourhood of a Solid," *Journal of Fluid Mechanics,* vol. 47, p. 283–290, 1971.

[34] P. A. Lush, "Impact of a Liquid Mass on a Perfectly Plastic Solid," *Journal of Fluid Mechanics,* vol. 135, pp. 373-387, 1983.

[35] R. Fortes-Patella, J. L. Reboud and L. Briancon-Marjollet, "Aphenomenological And Numerical Model For Scaling The Flowagrssiveness In Cavitation Erosion," in *Workshop on Cavitation Erosion*, Val de Reuil, 2004.

[36] M. Dular and A. Osterman, "Pit Clustering in Cavitation Erosion," *Wear,* vol. 265, pp. 811-820, 2008.

[37] M. Dular, B. Bachert, B. Stoffel and B. Sirok, "Relationship between Cavitation Structures and Cavitation Damage," *Wear,* vol. 257, pp. 1176-1184, 2004.

[38] E. Bennett and A. Ivanschenko, "Simcenter STAR-CCM+: Enabling MSI to Analyze Complex Pump Hydraulics," Star-CCM+, 2017.

[39] J. Sauer, "Instationaer kavitierende Stroemungen - Ein neues Modell, basierend auf Front Capturing VOF und Blasendynamik," Universitaet Kalrsruhe, Karlsuhe, 2000.

[40] M. Plesset and P. Epstein, "On the stability of gas bubbles in liquid-gas solutions," *Journal of Chemical Physics,* vol. 18, no. 11, 1985.

[41] B. Bachert, G. Ludwig, B. Stoffel, B. Sirok and M. Novak, "Experimental Investigations Concerning Erosive Aggressiveness Of Cavitation In A Radial Test Pump With The Aid Of Adhesive Copper Films," in *Fifth International Symposium on Cavitation*, Osaka, 2003.

[42] I. B. Celik, "Journal of Fluids Engineering Editorial Policy Statement on the Control of Numerical Accuracy," West Virginia University, Morgantown, 2005.

